Available online at www.sciencedirect.com
ScienceDirect
Applied Surface Science 254 (2008) 1997–2002
applied surface science
www.elsevier.com/locate/apsusc

Berkovich nanoindentation and deformation mechanisms in GaN thin films

Chien-Huang Tsai [a], Sheng-Rui Jian [b,*], Jenh-Yih Juang [c]

[a] Department of Automation Engineering, Nan Kai Institute of Technology, Nantou 54243, Taiwan
[b] Department of Materials Science and Engineering, I-Shou University, Kaohsiung 840, Taiwan
[c] Department of Electrophysics, National Chiao Tung University, Hsinchu 300, Taiwan

Received 5 July 2007; received in revised form 6 August 2007; accepted 6 August 2007
Available online 14 August 2007

Abstract

The deformation mechanisms of GaN thin films obtained by metal-organic chemical vapor deposition (MOCVD) method were studied using nanoindentation with a Berkovich diamond indenter, micro-Raman spectroscopy and the cross-sectional transmission electron microscopy (XTEM) techniques. Due to the sharpness of the tip of Berkovich indenter, the nanoindentation-induced deformation behaviors can be investigated at relatively lower load and, hence, may cover wider range of deformation-related phenomena over the same loading range. The load–displacement curves show the multiple ''pop-ins'' during nanoindentation loading. No evidence of nanoindentation-induced phase transformation and cracking patterns were found up to the maximum load of 300 mN, as revealed from the micro-Raman spectra and the scanning electron microscopy (SEM) observations within the mechanically deformed regions. In addition, XTEM observation performed near the cross-section of the indented area revealed that the primary deformation mechanism in GaN thin film is via propagation of dislocations on both basal and pyramidal planes. The continuous stiffness measurement (CSM) technique was used to determine the hardness and Young's modulus of GaN thin films. In addition, analysis of the load–displacement data reveals that the values of hardness and Young's modulus of GaN thin films are 19 ± 1 and 286 ± 25 GPa, respectively.

PACS : 62.20.−x; 68.37.Hk; 68.37.Lp; 81.15.Gh

Keywords: MOCVD; GaN; Nanoindentation; Multiple pop-ins; Micro-Raman spectroscopy; Focused ion beam; Transmission electron microscopy

1. Introduction

Gallium nitride (GaN) has been an intensively studied material over the last decade owing to its highly expected application potential in short-wavelength optoelectronic devices, semiconductor lasers and optical detectors [1–4]. The large band gap, strong inter-atomic bonding and associated high thermal conductivity are the main features making it an ideal material for high-temperature, high-power optoelectronic device applications. Consequently, majority of researches on this compound have been focused on exploring its optoelectronic characteristics. However, due to the ubiquitously existent lattice mismatch-induced stress between GaN thin films and the available substrates, the resultant defects have been found to significantly affect the threshold power density in stimulated emission of GaN optoelectronic devices [5]. Therefore, it is becoming increasingly evident that research on the mechanical characterizations of GaN thin films is equally important in order to harvest the most out of this fascinating material.

Mechanical properties of materials are size-dependent. A precise measurement of the mechanical properties of materials is required to use them as structural/functional elements in devices. Over the last two decades conventional nanoindentation has become a versatile technique for probing the mechanical properties of materials with characteristic dimensions in sub-micron regime [6–12]. In particular, the load–displacement curves obtained from the nanoindentation testing often provide pivotal information for properties, such as creep resistance [11], strain-rate sensitivity [11,13], fracture toughness and adhesion [14]. In addition, the shape of the load–displacement curves also

* Corresponding author.
E-mail address: srjian@gmail.com (S.-R. Jian).

0169-4332/$ – see front matter © 2007 Elsevier B.V. All rights reserved.
doi:10.1016/j.apsusc.2007.08.022

vividly reveals the various structural changes taking place within the indented materials during nanoindentation. For example, the onset for dislocation slip or twinning in InP and GaAs [15] and, the solid-state phase transformation in Si [16] and Ge [17] has been found to intimately correlate with the discontinuities appeared on the load–displacement curve during nanoindentation. Recently, Bradby et al. [18–20] investigated the mechanical deformation behaviors of GaN thin films using the spherical indenter with a radius of ~4 μm. During nanoindentation, a discontinuity (so-called "pop-in" event) in the loading curve was observed and the primary deformation mechanism in nanoindented GaN was attributed to slip nucleation [20]. Moreover, their results also indicated that no pressure-induced phase transformation was involved with the maximum indentation load applied (250 mN).

Herein, in the present study, we explored the deformation characteristics and the corresponding microscopic mechanism of the metal-organic chemical vapor deposition (MOCVD) grown GaN thin films with a three-side pyramidal Berkovich diamond indenter. The use of the Berkovich indenter not only will reflect the more realistic situations that might be encountered in real applications but also will result in much higher local pressure with similar load, and hence, will be helpful in clarifying the issue of pressure-induced phase transformation [21]. The micro-Raman spectroscopy examined near the indented regions indicated no phase transition was induced for load up to 300 mN and, as revealed by using cross-sectional transmission electron microscopy (XTEM), the deformation was primarily prevailing by dislocations slipping on both the basal and the pyramidal planes.

2. Experimental details

GaN thin films with average thickness of 2 μm were grown on the sapphire (0 0 0 1) substrate by MOCVD with the detailed growth procedures previously reported [7]. The mechanical properties of GaN thin films were characterized by means of a MTS NanoXP® (MTS Cooperation, Nano Instruments Innovation Center, TN, USA). The nanoindentation measurements, using a three-side pyramidal Berkovich diamond indenter of 50 nm radius (faces 65.3° from vertical axis), were conducted under the continuous stiffness measurement (CSM) procedures [22], which was accomplished by superimposing a small oscillation on the primary loading signal and, analyzing the resulting response of the system by using a lock-in amplifier. Prior to real measurement, the indenter was loaded and unloaded three times to ensure that the tip was properly in contact with the surface of GaN thin films and that any parasitical phenomenon is released from the measurement. At the fourth time, the indenter was loaded at a strain rate of 0.05 s^{-1} until reaching an indent depth (h_c) of 100 nm and was held for 30 s. Then, it was withdrawn with the same strain rate until 10% of the peak load was reached. At least 10 indents were performed on each sample. Each indentation was separated by 50 μm to avoid possible interferences between neighboring indents. We also followed the analytic method proposed by Oliver and Pharr [6] to determine the hardness and Young's modulus of GaN thin films from the load–displacement results. In this way, hardness and Young's modulus were obtained as a continuous function of penetration depth.

For microstructure analyses, a 10 × 3 indent array with each indent separated by 100 μm was produced by holding at the peak load of 300 mN for 30 s with the same loading/unloading rate of 10 mN/s. It was then characterized using a Ramanscope 2000 (Renishaw, UK) equipped with a charge coupled device (CCD) detector to detect possible phase changes within the indented regions. An argon ion laser operating at the excitation wavelength of 514.5 nm was used for Raman analysis. The incoming light was focused on the surface using a microscope objective lens of 100× and the scattered light was collected using the same objective lens. The beam intensity was kept at

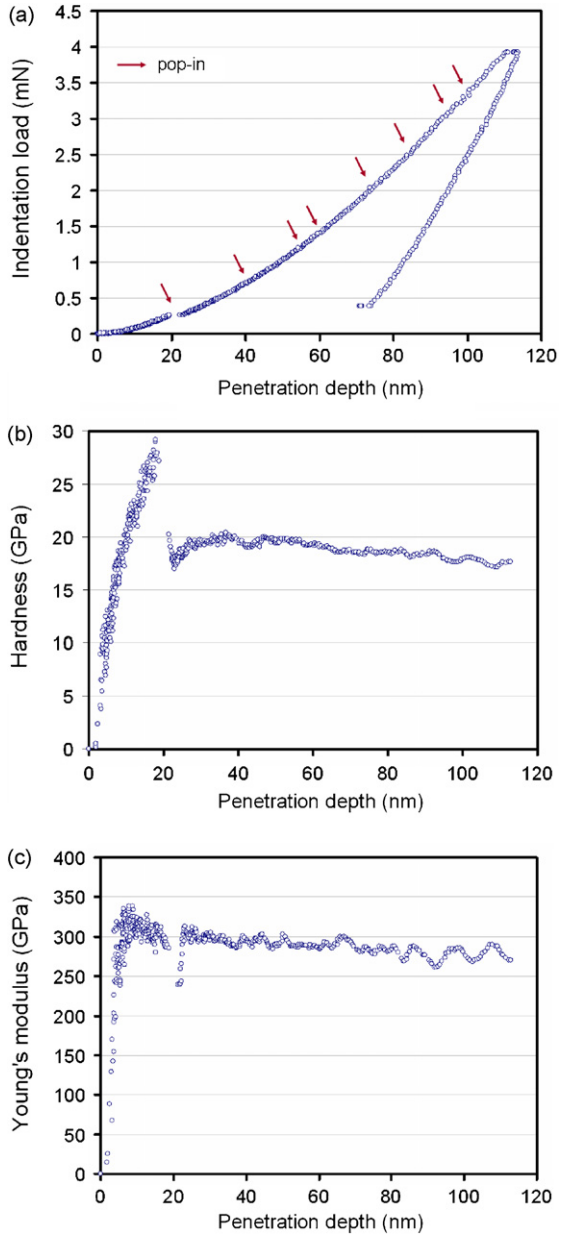

Fig. 1. Nanoindentation test results: (a) a typical load–displacement curve; (b) hardness–displacement curve; (c) Young's modulus–displacement curve for GaN thin film.

about 50 mW/cm^2 to avoid artifacts resulted from laser heating. Since the size of nanoindents and the spot size of the laser probe were both around 1 μm, the Raman spectra inevitably contained spectral features of the pristine surface outside the indentation region. The cross-sectional transmission electron microscopy (XTEM) samples were prepared by using a FEI Nova 220 Dual-Beam workstation—focused ion beam (FIB)/scanning electron microscopy (SEM) system. This technique enabled us to cut through the nanoindentation and locate the specific site of interesting efficiently. In practice, we first milled two crosses alongside the indented area for markers and, then deposited a 1 μm-thick Pt layer to protect this area of interest from Ga^+ ion beam damage and implantation. Material was removed from both sides of the selected area with an ion current of 5 nA, followed by successive thinning steps with decreasing current ranging from 3 nA to 300 pA until the lamella was about 1 μm-thick. Subsequently, the bottom and one side of the lamella were cut free while titling the sample at an angle of 45° to the ion beam. A central area containing the nanoindentation apex of a few micrometers in length was then chosen and thinned further to a thickness of ~100 nm, leaving at the sides, thicker areas that prevented the lamella from collapsing. An ion dose of 70 pA was adopted for final cleaning steps. Finally, a small area of interest was selected and thinned until electron transparency was achieved. The transfer of the lamella from the sample holder to a holey carbon-coated TEM grid was made *ex situ* by means of a shape glass tip under an optical microscope outside FIB station. A JEOL-2010 TEM operated at an accelerating voltage of 200 kV was used to investigate the microstructures of the XTEM lamella.

3. Results and discussion

The results of nanoindentation measurements are displayed in Fig. 1. Fig. 1(a) displays the typical load–displacement curve of GaN thin film obtained using the three-side pyramidal Berkovich diamond indenter. The hardness and Young's modulus of GaN thin films were calculated from the load–displacement data followed the analytic method developed by Oliver and Pharr [6]. The hardness is estimated from

$$H = \frac{P_{\max}}{A}, \tag{1}$$

where $P_{\max}$ is the maximum indentation load and the projected contact area A is the cross-sectional area of the indenter for a particular contact depth. For a perfect Berkovich indenter, it is given by

$$A = 24.56\, h_c^2. \tag{2}$$

However, indenters used in practical nanoindentation testing may deviate from the ideal shape due to blunting of the tip. The actual function $A(h_c)$ was obtained with a calibration procedure, as described in previous studies [6,22].

The elastic modulus is determined from the relation

$$E_r = \frac{1}{2\beta} S \sqrt{\frac{\pi}{A}} \tag{3}$$

where S is the measured stiffness and β is a shape constant of 1.034 for a Berkovich indenter. E_r is the effective elastic modulus defined by

$$\frac{1}{E_r} = (1 - v_f^2)\frac{1}{E_f} + (1 - v_i^2)\frac{1}{E_i} \tag{4}$$

The elastic modulus E_i and the Poisson's ratio v_i of the Berkovich indenter used in this work are 1141 GPa and 0.07 [6], respectively. Poisson's ratio v_f of the GaN thin films is taken as 0.25 [23]. Combining Eqs. (3) and (4), one can obtain the expression of Young's modulus E_f for GaN thin films, as following:

$$E_f = \frac{SE_i(1 - v_f^2)\sqrt{\pi}}{2\beta E_i\sqrt{A} - S(1 - v_i^2)\sqrt{\pi}} \tag{5}$$

The displacement dependence of the hardness and Young's modulus can be obtained from the CSM measurements, as illustrated in Fig. 1(b and c). The hardness and Young's modulus of GaN thin films are determined to be 19 ± 1 and 286 ± 25 GPa, respectively. The present results are largely in agreement with the previous studies on GaN thin films [19,20], except that the values of the mechanical parameters are slightly larger than those obtained by different measuring methods. Table 1 displays some of the relevant data for comparison [23–27]. We believe that the discrepancies among the mechanical parameters obtained by various indentation methods are mainly due to the specific tip–surface contact configuration and stress distribution inherent to each type of indenter tip.

Turning back to the load–displacement curve displayed in Fig. 1(a), it is evident that there exist multiple discontinuities along the loading course (indicated by the arrows) and is reflecting the process of plastic deformation in the material. These features are generally referred as ''pop-ins'' associated with hexagonal materials and were attributed to nucleation of additional slip bands [20,28,29]. Nevertheless, we note that, in the present case, the threshold load and the indentation depth for the first ''pop-in'' appear to take place at much smaller values as compared to those reported by Bradby and co-workers [18] for GaN films. The origin of this discrepancy is presumably due to the fact that in the present study the pyramidal (Berkovich) indenter rather than the spherical one was used. In the former, the sharp tip may have resulted in much higher stress at the same load. It is noted that, in Fig. 1(b), the contact pressure (or Meyers hardness) increases with the indenter penetration depth to an unusual high value and followed by a sudden precipitous drop when the first pop-in event at h_c ~20 nm took place and the subsequent pop-in events only resulted in relatively small hardness oscillations around 19 ± 1 GPa. On the other hand, the value of Young's modulus, shown in Fig. 1(c), is not affected significantly prior to the first pop-in event at h_c ~20 nm. It then displayed a sudden drop over the same range of indent depth wherein the softening occurs and remains relatively constant at 286 ± 25 GPa afterward. The qualitative features of these behaviors are similar to those reported in the literature for various compound semiconductors and are generally attributed to the effects of slip band

Table 1
Hardness and Young's modulus of GaN thin films obtained from various measurement methods

	GaN samples	H (GPa)	E_f (GPa)	Indenter tip
Drory et al. [23]	As-grown	12 ± 2	287	Vickers
Nowak et al. [24]	As-grown	20	295	Spherical
Kucheyev et al. [19]	As-grown	13.4	233	Spherical
	Ion-damaged	15.1	164	
	Amorphized	2.4	65	
Jian et al. [7]	As-grown	19.34 ± 2.13	314.93 ± 40.58	Berkovich
	Si-doped	20.12 ± 2.51	247.16 ± 14.89	
Jian et al.[a]	As-grown	19 ± 1	286 ± 25	Berkovich
Navamathavan et al. [25]	As-grown	22.5	–	Berkovich
Fujikane et al. [26]	As-grown	17	320	Berkovich
Kavouras et al. [27]	As-grown	13.67 ± 0.15	–	Knoop
	O-doped	14.75 ± 0.22	–	
	Mg-doped	16.87 ± 0.13	–	
	Au-doped	12.16 ± 0.09	–	
	Xe-doped	11.35 ± 0.12	–	
	Ar-doped	9.98 ± 0.14	–	

[a] This study.

nucleation due to stress-induced dislocation "pop-ins" [15,19,20]. However, in the present case, the threshold has occurred at a much smaller indenter penetration. Assuming the same threshold stress is required to induce pop-in dislocations, this result implies that the deformation in our sample is taking place in an area of about two orders of magnitude smaller than those obtained with the spherical indenters.

In order to take the advantage of using a sharper indenter tip to resolve whether or not pressure-induced phase transformation can occur in compound semiconductors, we also conducted experiments with a much higher indentation load and deeper indentation. Fig. 2 shows the typical results obtained with a maximum load of 300 mN and penetration depth of 800 nm. Similar features of multiple pop-ins are observed. However, a closer look at the loading curves displayed in Figs. 1(a) and 2 reveals that the multiple pop-ins do not exactly coincide at the same indenter penetration depths. Since each curve is

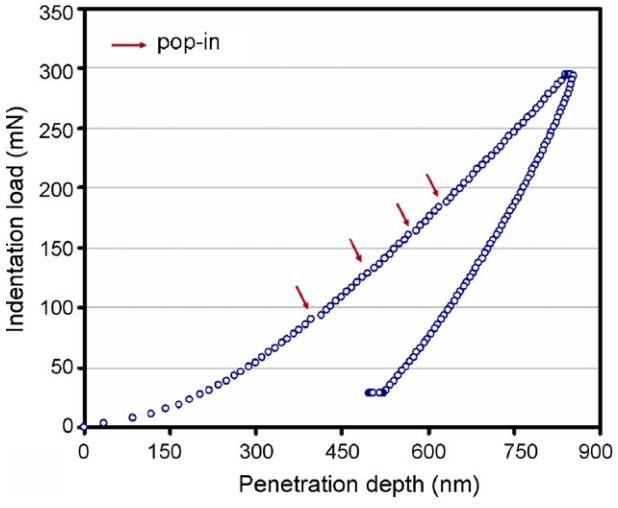

Fig. 2. Typical continuous load–displacement curve for GaN films obtained by using Berkovich indentation. The maximum load was 300 mN.

associated with different stress rates depending on the maximum indentation load, suggesting that the first pop-in event is not thermally activated. These phenomena have been frequently attributed to mechanisms such as dislocation nucleation [30–32], or formation of micro-cracks [28,33]. In addition, the no reversal discontinuities during unloading curve, commonly called "pop-out" events, were observed here; such phenomena were observed for instance in silicon and related to phase transformation just beneath the diamond indenter [16].

The multiple pop-ins behavior has been observed in materials with hexagonal structures such as sapphire [34], GaN [20] and single-crystal bulk ZnO [29], while for materials like InP and GaAs with the cubic structure only single pop-in event was observed [15]. To delineate the possible mechanisms responsible for these differences, we first look for the apparent evidences at the indented surfaces. The inset of Fig. 3 shows the typical SEM micrograph for an indented surface obtained with the maximum applied load of 300 mN. There is no evidence of dislocation activity or crack formation in the area of the indented surface. Thus, if the dislocation nucleation and subsequent propagation are indeed the primary mechanism for the observed multiple pop-ins, it should prevail underneath the indented surface. It is also interesting to check if there is any pressure-induced phase transformation involved.

At the ambient conditions, GaN tends to crystallize into the Wurtzite structure. Nevertheless, it has been theoretically predicted [35,36] and experimentally confirmed [37–39] that, upon applying a hydrostatic pressure on the order of about 50 GPa, GaN will undergo the pressure-induced phase transformation into the Rocksalt structure. These values are significantly higher than the apparent room-temperature hardness of GaN thin films and the maximum load employed in this study. As will be presented in the followings, we used the micro-Raman spectroscopy and XTEM techniques in trying to clarify some of the issues concerning the nanoindentation-induced phase transformation in this material. The micro-Raman spectra

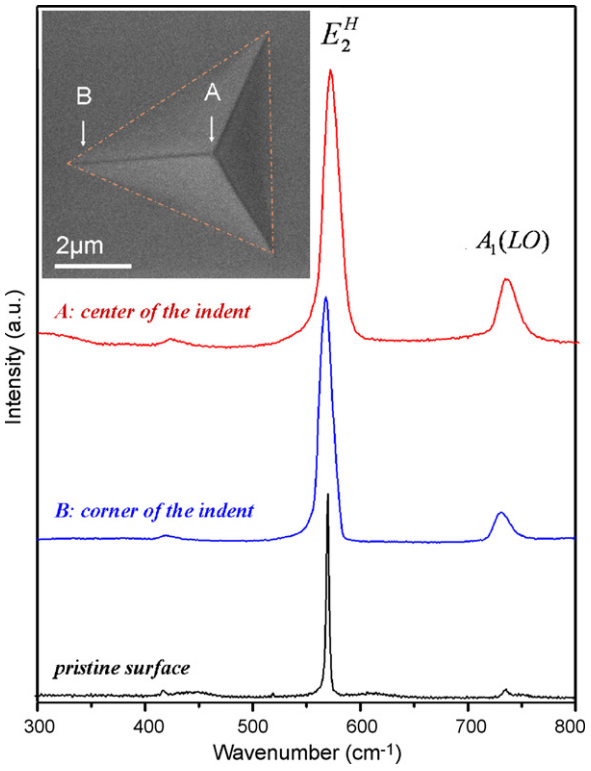

Fig. 3. The Raman spectra of GaN thin film taken on the pristine surface and after nanoindentation (at the corner and center of the indent). Changes in Raman spectra after indentation, though displaying the effects of compressive stress, do not show clear evidence of phase transformation. The inset shows the SEM micrograph of the same area after the Berkovich indentation on GaN thin film obtained at an indentation load of 300 mN. No cracking is evident to be responsible for the multiple pop-ins observed in the load–displacement curves.

for Berkovich indenter operated at an indentation load of 300 mN are illustrated in Fig. 3. Three spectra are displayed—one before nanoindentation and the other two taken at different positions (corner and center of indent) after nanoindentation. The characteristic features of E_2^H and A_1(LO) peaks, locating, respectively, at 568 and 733 cm^{-1} are clearly observed in the pristine GaN thin film. As is evident from Fig. 3, both E_2^H and A_1(LO) modes are shifted to the higher wavenumbers after indentation. The fact that the peak displacement is largest at the center of the indented area and decreases outward indicates that the compressive stresses might be the dominant factors. In addition, band broadening is revealed due to residual deformation via nanoindentation. We note that Puech et al. [40] also reported the similar shifts in micro-Raman results taken from point-indentation with an indentation load of 100 mN and had attributed these small shifts to residual compressive stress within the indented area. Finally, no extra peaks were observed in our micro-Raman spectra from nanoindentation, indicating that no phase transition in the material has occurred. Furthermore, the SEM image of the same indentation area displayed in the inset of Fig. 3 does not reveal any characteristic of the pressure-induced metallization, either. We suspect that, in the film–substrate system, the indentation load applied to the film may have been partly absorbed by the substrate and distributed over a much larger area. Consequently, the local stress concentration beneath

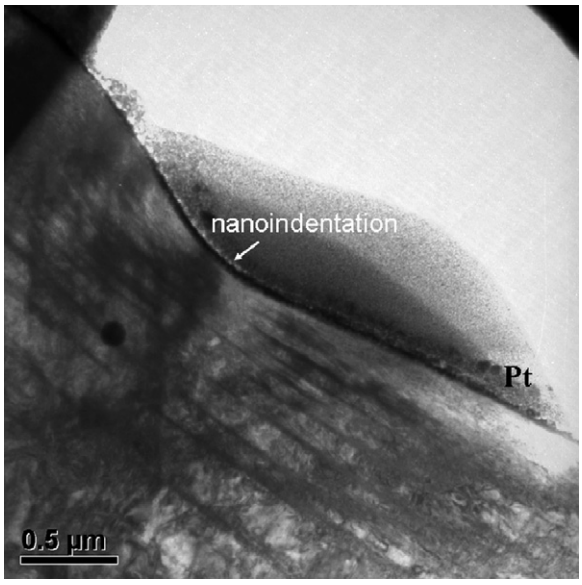

Fig. 4. A bright-field XTEM image in the vicinity immediately under the Berkovich indent applied on the GaN thin film with an indentation load of 300 mN.

the indenter is significantly reduced to values insufficient for phase transformation to occur.

To further elucidate the nanoindentation-induced deformation, a bright-field XTEM image of an indentation load of 300 mN in GaN thin films is displayed in Fig. 4. While extensive deformation-induced damage is evident directly underneath the Berkovich indenter, there is no evidence of cracking in the GaN thin films. Instead, it can be seen that the dislocations gliding along the pyramidal $\{1\,0\,\bar{1}\,1\}$ planes interact heavily with the slip bands propagating along the (0 0 0 1) basal plane orientation. Since the propagation of dislocations along the pyramidal planes oriented at an angle of ~60° to the sample surface and are likely to interact with those gliding along the basal planes, it might be the primary mechanism giving rise to the multiple pop-ins during loading. Alternatively, the interactions between the gliding dislocations and the pre-existing defects (e.g. the threading dislocations) in GaN thin films may also play a role. From the above experimental observations of micro-Raman and XTEM analyses, it is suggestive that the predominated nanoindentation-induced deformation mechanism in GaN thin films is associated with dislocation generation and propagation instead of phase transition, despite the fact that the GaN thin films had undergone severe plastic deformation. These results are in contrast to those reported by Weyher et al. [21], in that phase transformation had been identified as the primary deformation mechanism in GaN based on the detection of polycrystalline phases in the vicinity of indented area after a Vickers indentation carried out at a very high load of 2 N.

From the above discussions, it appears that the occurrence of multiple pop-ins is mainly related to the formation and propagation of dislocations. In the current case, there are, at least, three possible mechanisms that are responsible for this phenomenon. Firstly, the specific hexagonal lattice structure of GaN offers the possibility of interactions between dislocations

gliding along the pyramidal and basal planes. Secondly, the usual ''slip-stick'' behavior [20] can also prevail by the interactions between the as-grown dislocations and that are being punched out by nanoindentation loading. Finally, it could be just a consequence of punching out of the threading dislocations by nanoindentation. In other words, the threading dislocations originally existing in the GaN thin films could, respectively, display sudden propagations when acquired enough threshold energy from the deformation, resulting in the multiple pop-ins. The fact that multiple pop-ins were observed only in hexagonal materials strongly suggests that the first mechanism might be of primary importance.

4. Conclusions

To summarize, details of nanoindentation-induced mechanical deformation of the GaN thin films fabricated by MOCVD method have been investigated by using nanoindentation with a Berkovich diamond indenter, Raman micro-spectroscopy and XTEM techniques. The multiple pop-ins was found in the load–displacement curve on loading, while no pop-out was observed during the unloading course. According to the observations of micro-Raman and XTEM, the nanoindentation-induced mechanical deformation is due primarily to the generation and propagation of dislocations gliding along the pyramidal and basal planes specific to the hexagonal structure of GaN rather than by indentation-induced phase transformations. The cracking-induced effects on multiple pop-ins were evidently ruled out in the current case, as well.

Acknowledgements

This work was partially supported by the National Science Council of Taiwan, under Grants: NSC 95-2112-M-009-035-MY3 and NSC 96-2112-M-009-017. Authors would like to thank Prof. X.D. Li, Department of Mechanical Engineering, University of South Carolina, USA, for his helpful revisions and suggestions.

References

[1] F.A. Ponce, D.P. Bour, Nature 386 (1997) 351.
[2] S. Nakamura, S.J. Pearton, G. Fasol, The Blue Laser Diode Laser, Springer, Berlin, 2000.
[3] T. Miyajima, T. Yojyo, T. Asano, K. Yanashima, S. Kijima, T. Hino, M. Takeya, S. Uchida, S. Tomiya, K. Funato, T. Asatuma, T. Kobayashi, M. Ikeda, J. Phys.: Condens. Matter 13 (2001) 7009.
[4] M. Mikulics, M. Marso, P. Javorka, P. Kordoš, H. Lüth, M. Kočan, A. Rizzi, S. Wu, R. Sobolewski, Appl. Phys. Lett. 86 (2005) 211110.
[5] K. Funato, F. Nakamura, S. Hashimoto, M. Ikeda, Jpn. J. Appl. Phys. 37 (1998) L1023.
[6] W.C. Oliver, G.M. Pharr, J. Mater. Res. 7 (1992) 1564.
[7] S.R. Jian, T. Fang, D.S. Chuu, J. Electron. Mater. 32 (2003) 496.
[8] X.D. Li, H.S. Gao, C.J. Murphy, L. Gou, Nano Lett. 4 (2004) 1903.
[9] X.D. Li, X. Wang, Q. Xiong, P.C. Eklund, Nano Lett. 5 (2005) 1982.
[10] H. Ni, X.D. Li, Nanotechnology 17 (2006) 3591.
[11] S.R. Jian, T. Fang, D.S. Chuu, Appl. Surf. Sci. 252 (2006) 3033.
[12] S.Y. Chang, T.K. Chang, J. Appl. Phys. 101 (2007) 033507.
[13] X. Ma, F. Yoshida, Appl. Phys. Lett. 82 (2003) 188.
[14] A.A. Volinsky, W.W. Gerberich, Microelectron. Eng. 69 (2003) 519.
[15] J.E. Bradby, J.S. Williams, J.W. Leung, M.V. Swain, P. Munroe, Appl. Phys. Lett. 78 (2001) 3235.
[16] X.Q. Yan, X.M. Huang, S. Uda, M.W. Chen, Appl. Phys. Lett. 87 (2005) 191911.
[17] J. Jang, M.J. Lance, S. Wen, G.M. Pharr, Appl. Phys. Lett. 86 (2005) 131907.
[18] S.O. Kucheyev, J.E. Bradby, J.S. Williams, C. Jagadish, M. Toth, M.R. Phillips, M.V. Swain, Appl. Phys. Lett. 77 (2000) 3373.
[19] S.O. Kucheyev, J.E. Bradby, J.S. Williams, C. Jagadish, M.V. Swain, G. Li, Appl. Phys. Lett. 78 (2001) 156.
[20] J.E. Bradby, S.O. Kucheyev, J.S. Williams, J.W. Leung, M.V. Swain, P. Munroe, G. Li, M.R. Phillips, Appl. Phys. Lett. 80 (2002) 383.
[21] J.L. Weyher, M. Albrecht, T. Wosinski, G. Nowak, H.P. Strunk, S. Porowski, Mater. Sci. Eng. B 80 (2001) 318.
[22] X.D. Li, B. Bhushan, Mater. Charact. 48 (2002) 11.
[23] M.D. Drory, J.W. Ager III, T. Suski, I. Grzegory, S. Porowski, Appl. Phys. Lett. 69 (1996) 4044.
[24] R. Nowak, M. Pessa, M. Suganuma, M. Leszczynski, I. Grzegory, S. Porowski, F. Yoshida, Appl. Phys. Lett. 75 (1999) 2070.
[25] R. Navamathavan, Y.T. Moon, G.S. Kim, T.G. Lee, J.H. Hahn, S.J. Park, Mater. Chem. Phys. 99 (2006) 410.
[26] M. Fujikane, M. Leszczyński, S. Nagao, T. Nakayama, S. Yamanaka, K. Niihara, R. Nowak, J. Alloys Compd. 450 (2008) 405.
[27] P. Kavouras, Ph. Komninou, Th. Karakostas, Thin Solid Films 515 (2007) 3011.
[28] T.F. Page, W.C. Oliver, C.J. Mc Hargue, J. Mater. Res. 7 (1992) 469.
[29] S.O. Kucheyev, J.E. Bradby, J.S. Williams, C. Jagadish, M.V. Swain, Appl. Phys. Lett. 80 (2002) 956.
[30] D.F. Bahr, D.E. Kramer, W.W. Gerberich, Acta Mater. 46 (1998) 3605.
[31] C. Tromas, J.C. Girard, V. Audurier, J. Woirgard, J. Mater. Sci. 34 (1999) 5337.
[32] A.J. Haq, P.R. Munroe, M. Hoffman, P.J. Martin, A. Bendavid, Thin Solid Films 515 (2006) 1000.
[33] S.J. Bull, J. Phys. D: Appl. Phys. 38 (2005) R393.
[34] R. Nowak, T. Sekino, S. Maruno, K. Niihara, Appl. Phys. Lett. 68 (1996) 1063.
[35] A. Munoz, K. Kunc, Phys. Rev. B 44 (1991) 10372.
[36] P.E. van Camp, V.E. van Doren, J.T. Devreese, Solid State Commun. 81 (1992) 23.
[37] P. Perlin, C.C. Jauberthie, J.P. Itie, A.S. Miguel, I. Grzegory, A. Polian, Phys. Rev. B 45 (1992) 83.
[38] H. Xia, Q. Xia, A.L. Ruoff, Phys. Rev. B 47 (1993) 12925.
[39] M. Ueno, M. Yoshida, A. Onodera, O. Shimomura, K. Takemura, Phys. Rev. B 49 (1994) 14.
[40] P. Puech, F. Demangeot, J. Frandon, C. Pinquier, M. Kuball, V. Domnich, Y. Gogotsi, J. Appl. Phys. 96 (2004) 2853.